Science Advances
AAAS

Supplementary Materials for

Inhibition of peptidoglycan synthesis is sufficient for total arrest of staphylococcal cell division

Jan-Samuel Puls *et al.*

Corresponding author: Fabian Grein, grein@uni-bonn.de

Sci. Adv. **9**, eade9023 (2023)
DOI: 10.1126/sciadv.ade9023

This PDF file includes:

Supplementary Text

Convolved Average Projections

Typical approaches to analyze fluorescence localization in bacteria often include preselection of cells within a sample (e.g., the analysis of septal:peripheral ratios can only be reliably performed on cells with the septal plane oriented in a 90° angle to the viewing plane). Combining the obtained microscopy images of all cells within a sample set into a comprehensive representation is a promising approach to visualize and analyze fluorescence localization patterns and changes thereof in an automated and unbiased way. Recent studies used such an approach by combining cells into average projections for analysis (*24*, *52*). However, this approach is unsuitable for the unique challenges of *S. aureus* morphology. Most model organisms (like *E. coli*, *B. subtilis, S. pneumoniae*) display some form of geometric asymmetry, which enables orientation of the image plane with respect to the cell morphology. However, *S. aureus* stays nearly spherical throughout the cell cycle (*29*), and the minor elongation is not sufficient to precisely detect the medial axis automatically in wavelength-limited fluorescence microscopy. Therefore, the multitude of different viewing angles on cells of *S. aureus* negatively impacts normal average projection attempts. We found that the method of average projection could be adapted by increasing the contrast of raw cell images via convolution. The resulting convolved average projections (CAPs) revealed the localization patterns of analyzed populations reliably.

To generate a CAP from a sample set, all individual cell images of the set are convolved to increase contrast, emphasize fluorescence maxima and minimize unspecific background. All cells with a distinguishable septum are rotated into a vertical orientation. All convolved and correctly oriented single cell images are then z-projected to a single average image (Fig. S1A). This convolved average projection visualizes general localization patterns within the complete sample population. This approach can be used to visualize localization of any signal in a cell population, given that cells have a similar shape.

We validated technical reproducibility throughout a range of input cell numbers (Fig. S1B,C,D) and biological reproducibility while testing the impact of different characteristic phenotypes on the final CAP image (Fig. S1E,F). We observed that both phenotypes contribute in a way that each can be quantitatively assessed individually by analysing CAP intensity values.

Overall, CAPs enable fast and unbiased automated procession of large cell data sets resulting in a condensed, comprehensive representation of substantial fluorescence localization patterns of the entire population. Preservation of relevant spatial information ensure that CAP images can be analysed with methods typically used for single cell analysis with the effect, that large data sets can be assessed easily to determine general localization trends for further detailed investigation.

Determination of antibiotic treatment time and concentration

To determine the appropriate antibiotic concentration and time range for observing the key cellular effects of vancomycin, telavancin and oxacillin on the cell division progress in *S. aureus*, we evaluated the antibacterial activity of the three antibiotics. Telavancin showed a notable inoculum effect in the minimal inhibitory concentration (MIC), therefore we optimized the experimental setups using a higher inoculum than described in the CLSI standard. Using the obtained MIC values of 2 µg/mL (vancomycin), 1 µg/mL (telavancin) and 0.5 µg/mL (oxacillin) we determined the killing kinetics of the antibiotics (Fig. S6). We found that a concentration of 4 x MIC for each antibiotic was suited for our purpose, as it resulted in long-term bactericidal impact while the moderate effects on cell viability within the first hour of treatment enabled us to investigate the cellular effects preceding ultimate cell death.

Impact of telavancin membrane interaction on Z-ring stability

Due to the described membrane depolarizing effect of telavancin (*53*), we investigated a putative disruption of Z-ring integrity caused by the lipoglycopeptide. After loss of the membrane potential, the GTPase activity of FtsZ is eliminated, resulting in depolymerization and disassembly of the Z-ring (*54*). However, we did not observe such an effect with either telavancin or vancomycin (Fig. S6A,B). As an additional control, we added the membrane depolarization probe $DiBAC_4(3)$ to the samples, whose fluorescence intensity increases proportional to membrane depolarization (*47*). Again, we could not observe any depolarizing effects of the glycopeptides. In contrast, 1 x MIC (16 µg/mL) nisin, a lantibiotic which binds to Lipid II and causes rapid membrane depolarization via pore formation (*55*) completely disintegrated Z-rings and increased $DiBAC_4(3)$ fluorescence massively in the same time (Fig. S6A,B). We additionally tested if vancomycin and telavancin release $DiSC_3(5)$, an auto-quenching dye which accumulates in cells and is released upon membrane depolarization resulting in an increase in fluorescence (*47*). Again, we found no signs of membrane depolarization caused by either compound (Fig. S6C). We concluded that no membrane depolarization effect would influence our visualization of Z-ring dynamics during treatment with telavancin within the concentration and time range of our experiments.

Original microscopy data availability

The Quantitative Biology Center (QBiC) at the University of Tübingen supports in storage and management of original microscopy data. The QBiC provides a private cloud environment using secure data sharing for scientific collaboration, via controlled access to the QBiC portal (https://portal.qbic.uni-tuebingen.de). Access will be granted upon request by sending an email mentioning the project identifier QDSKD to: support@qbic.zendesk.com

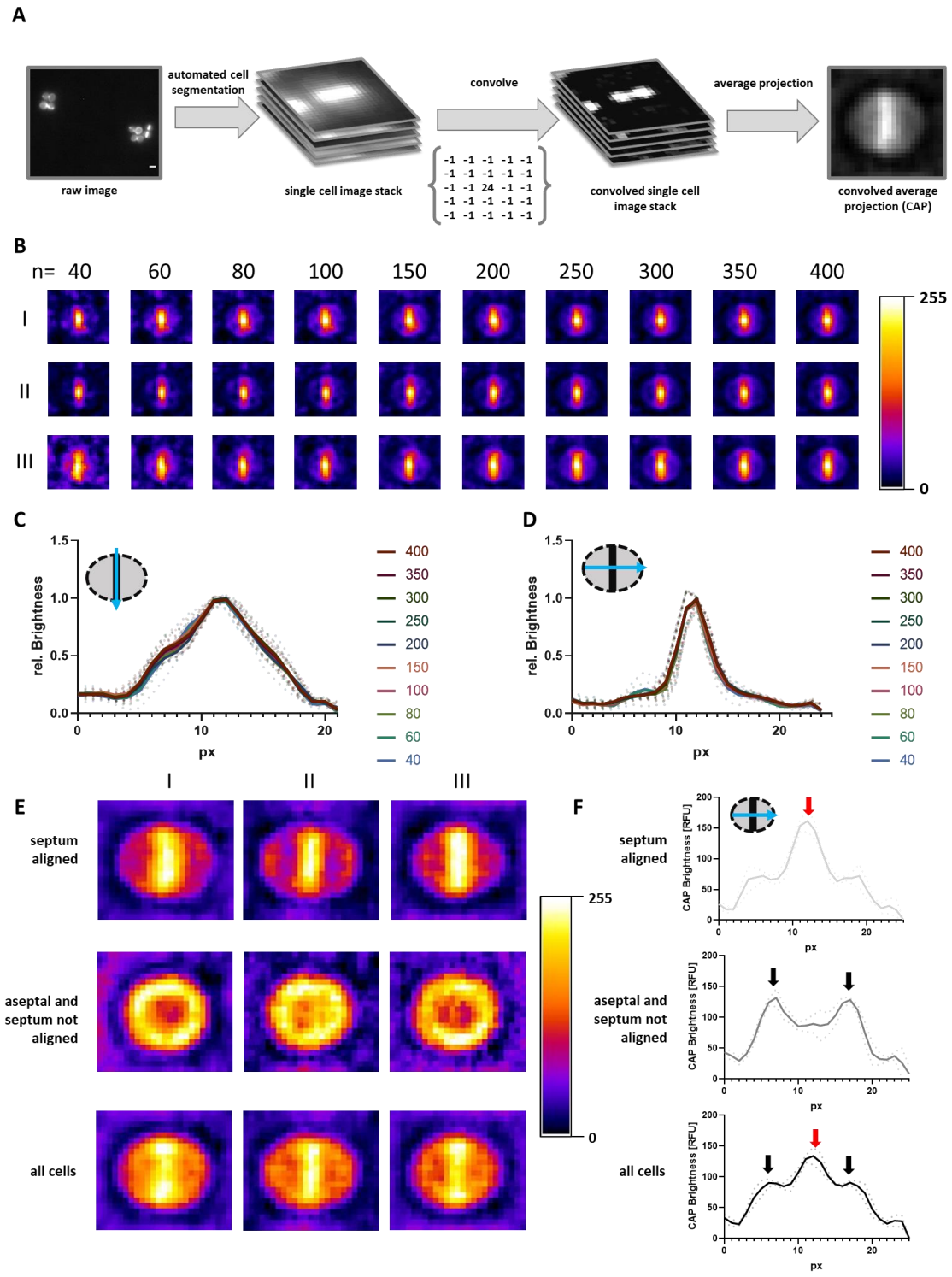

Fig. S1.

Convolved average projections are a tool for comprehensive representation of fluorescence localization within a population. **(A)** Schematic overview of the generation of convolved average projections. Automated cell segmentation and extraction of single cell images was performed using the ImageJ plugin MicrobeJ. **(B-D)** Technical reproducibility of CAPs and impact of cell

number used for CAP generation. **(B)** Technical replicates I - III of CAPs were generated from a sample population of 1292 cell of *S. aureus* RN4220 pCQ11-MurJ-mNeonGreen. For each technical replicate, a subsample of 400 cells was randomly chosen via the MicrobeJ random selection function. To test impact of cell number on CAP appearance, cells were stepwise subtracted from the subsample stack, with n corresponding to the number of cells left in the subsample. The order of individual cells in each technical replicate subsample stack was determined according to the MicrobeJ name.ID image naming. **(C)** Quantification of CAP Brightness of the technical replicates shown in **A** along the septal axis, plotted relative the medial brightness value. For each condition, the mean of three independent biological experiments is shown as thick line ± SD as dotted, semi-transparent lines. **(D)** Quantification of CAP brightness of the technical replicates shown in **A** along the medial axis, plotted relative the septal brightness value. For each condition, the mean of three independent biological experiments is shown as thick line ± SD as thin, semi-transparent lines. E-F: Representation of different localization patterns in CAP appearance. **(E)** Cells of three independent biological replicates (I – III) of *S. aureus* RN4220 pCQ11-FtsZ-SNAP (labelled with SNAP-Cell® TMR Star) were manually sorted for the visual appearance of a distinctive septal signal. CAPs were generated from both subpopulations individually and from the complete population. **(F)** Quantification of CAP Brightness of **E** along the medial axis. For each subpopulation, the mean of three independent biological experiments is shown as thick line ± SD as dotted, semi-transparent lines. The combined CAP of the complete sample population still conserves information about the subpopulations (red arrow: characteristic septal signal, black arrow: characteristic aseptal signal).

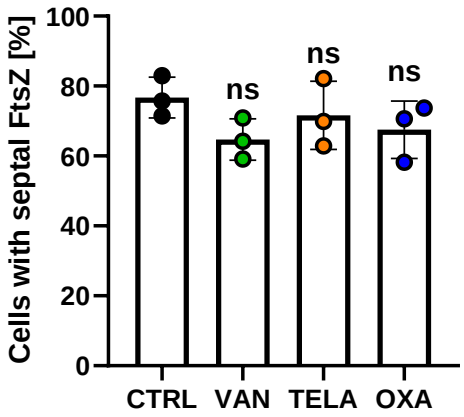

Fig. S2.

Relative abundance of cells with septal FtsZ localization as % of total population analyzed in Figure 1. Points correspond to values of individual replicates, bar shows the mean of three independent biological experiments ± SD. Number of individual cells per replicate are shown in Tab. S2 for all datasets. Statistical significance was determined against the untreated control with unpaired two-tailed students t-tests with a 95% confidence interval. Statistical significance was denoted as ns, not significant.

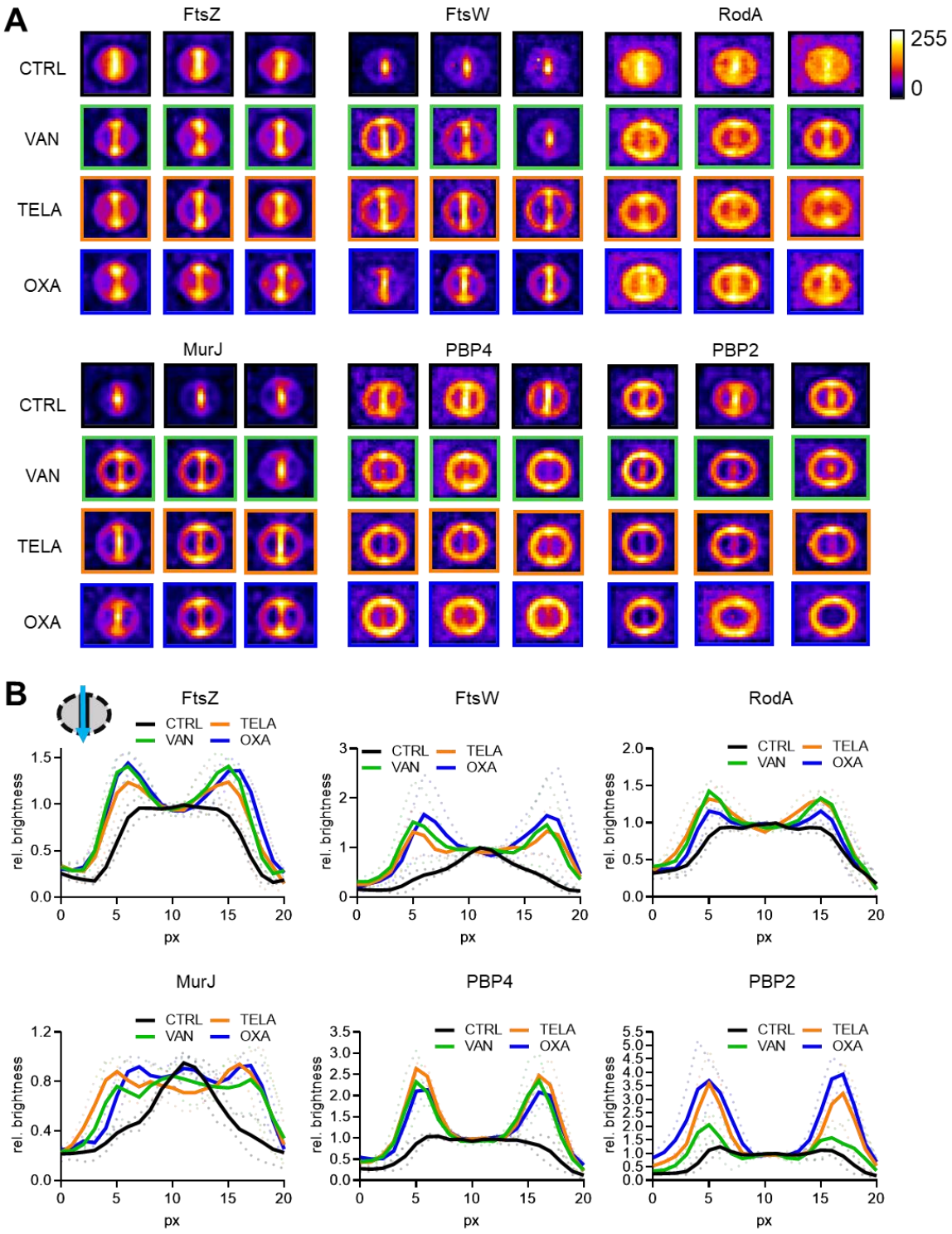

Fig. S3.

(A) CAPs of all individual biological experiments used for analysis in this study. **(B)** Quantification of CAP brightness for all CAPs shown in (A) along the septal axis, plotted relative to the medial brightness value. For each condition, the mean of three independent

biological experiments is shown as thick, full line. The respective standard deviations are given as dotted, semi-transparent lines. Number of individual cells per replicate are shown in Tab. S2 for all datasets.

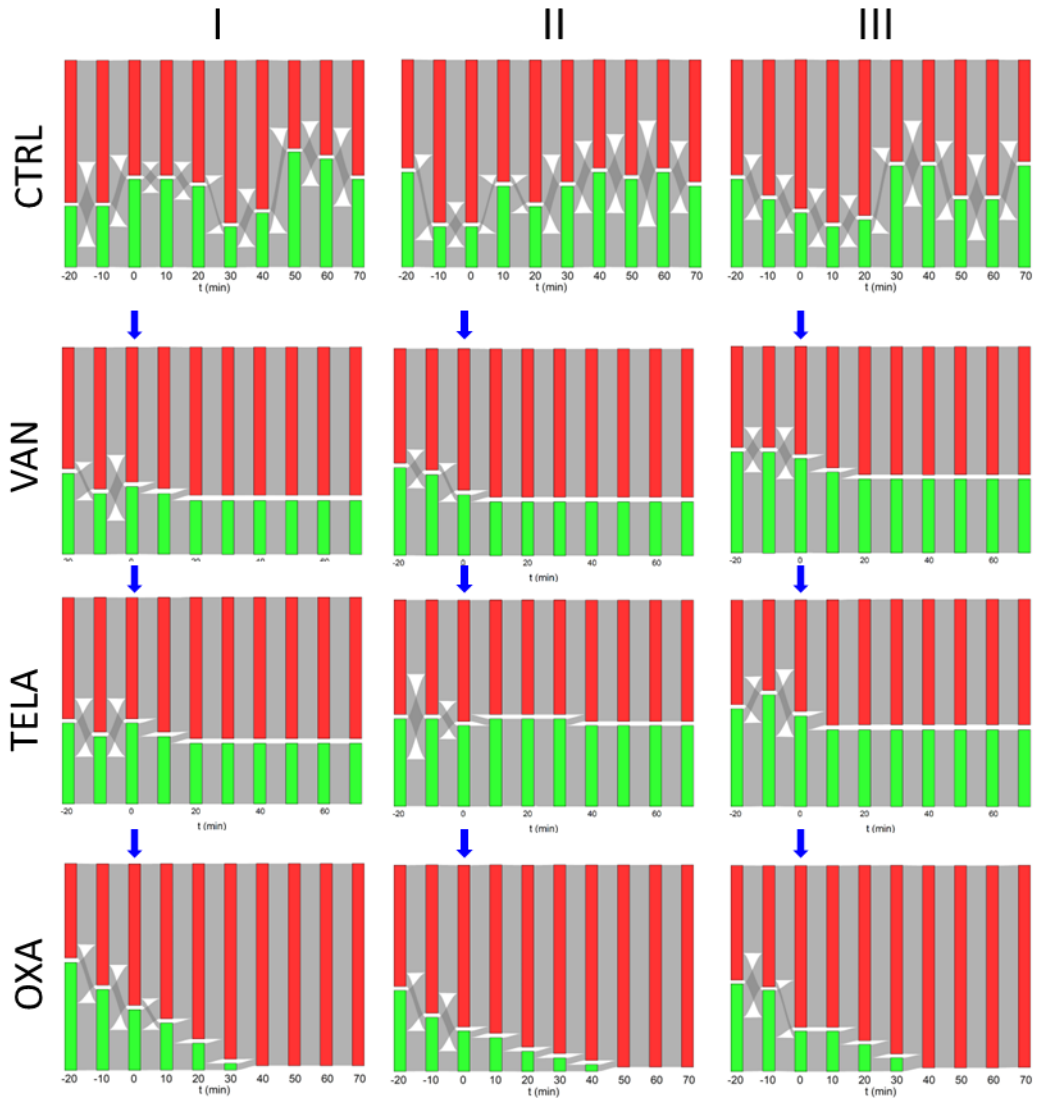

Fig. S4.

Individual biological replicates (I, II and III) of the mean PBP2 localization pattern dynamics. The time point of antibiotic addition is marked with a blue arrow. Red: cells without septal PBP2 localization. Green: cells with septal PBP2 localization. Red-to-green fluxes correspond to cells that recruit PBP2 to the septum. The green-to-red fluxes correspond to cells that divide and thereby lose septal PBP2 localization in daughter cells. Bar height represents relative abundance of cells with the respective PBP2 localization. Sum of both bars is always 100%. For each replicate and condition n = 30 were evaluated.

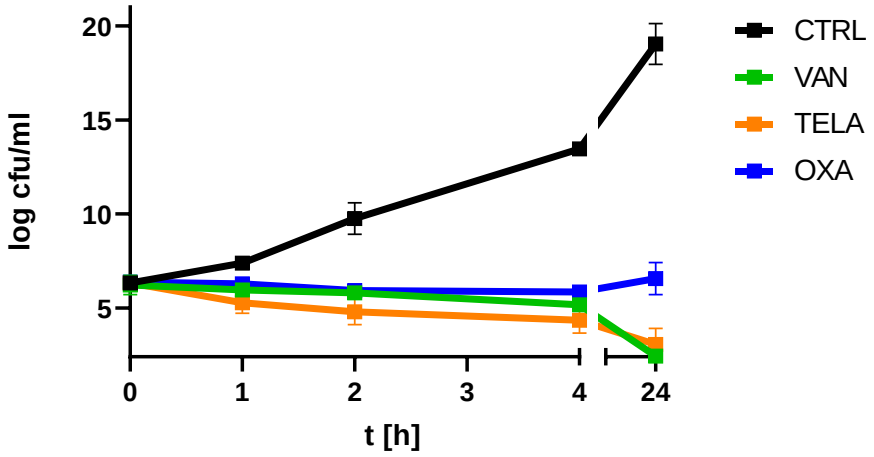

Fig. S5.

Killing kinetics of vancomycin, telavancin and oxacillin against *S. aureus* HG001. Lines show the mean of three independent biological experiments ± SD.

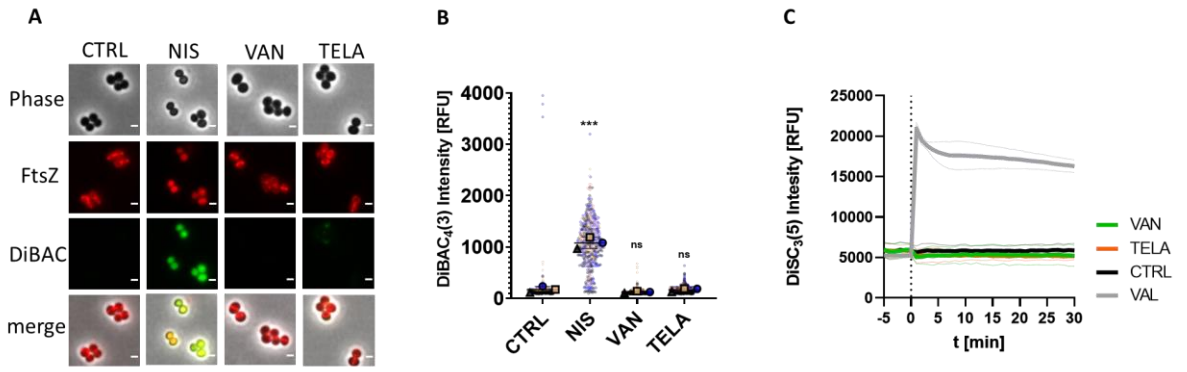

Fig. S6.

Glycopeptides telavancin and vancomycin do not affect the membrane potential at 4 x MIC. **(A)** Representative images of *S. aureus* RN4220 pCQ11-FtsZ-SNAP treated with 1 x MIC nisin (NIS) or 4 x MIC VAN or TELA for 25 min. Red: FtsZ-SNAP, SNAP-tag labelled with SNAP-Cell® TMR Star. Green: fluorescent membrane depolarization probe $DiBAC_4(3)$. Representative images of three independent biological experiments. **(B)** Quantification of $DiBAC_4(3)$ fluorescence intensities of individual cells. Small semitransparent points show individual cell data with colors corresponding to the individual biological experiment. Large points show the mean of each individual biological experiment. Line shows mean of three individual biological experiments ± SD.**(C)** Quantification of $DiSC_3(5)$ fluorescence during treatment with vancomycin, telavancin, and an untreated control. 5 µM valinomycin + 300 mM KCl was used as positive control. Mean of three independent biological experiments is shown as thick line ± SD as thin, semi-transparent lines. Number of individual cells per replicate are shown in Tab. S2 for all datasets. Statistical significance was determined against the untreated control with unpaired two-tailed students t-tests with a 95% confidence interval. Statistical significance was denoted as ns, not significant; ***, p = 0.001 to 0.0001.

Table S1.

Strains, plasmids and primers used in this study.

Strain	**Reference**	**Selective antibiotic**
S. aureus RN4220 wild type	(*56*)	-
S. aureus HG001 wild type	(*57*)	-
S. aureus RN4220 pCQ11-FtsZ-SNAP	(*19*)	10 µg/mL erythromycin
S. aureus RN4220 pCQ11-FtsZ-mCherry	this study	10 µg/mL erythromycin
S. aureus RN4220 pCQ11-MurJ-mNeonGreen	this study	10 µg/mL erythromycin
S. aureus RN4220 FtsW-GFPmut2	(*42*)	-
S. aureus RN4220 RodA-GFP	this study	-
S. aureus RN4220 FtsW-GFPmut2 pCQ11-FtsZ-SNAP	this study	10 µg/mL erythromycin
S. aureus RN4220 RNpPBP2-31	(*14*)	10 µg/mL erythromycin
S. aureus RN4220 pCQ11-PBP4-YFP	this study	10 µg/mL erythromycin
E. coli Stellar™	Takara Bio	-
Plasmid	**Reference**	**Information / Purpose**
pCQ11-FtsZ-SNAP	(*19*)	Visualization of FtsZ
pCQ11-FtsZ-mCherry	this study	Live-cell visualization of FtsZ
pCQ11-GFP	C. Quiblier & B. Berger-Bächi	backbone for pCQ11-mNeonGreen
pCQ11-mNeonGreen	this study	backbone for pCQ11-MurJ-mNeonGreen
pLOM-S-mNeongreen-EC18153	Addgene plasmid # 137075	*mNeongreen* template
pCQ11-MurJ-mNeonGreen	this study	MurJ with C-terminal mNeongreen fusion

Primer	**Sequence**	**Amplicon**
mNeon-for	TTATGCTAGCTTAACCCGGGATGGCGTCGAAGG	*mNeongreen*
mNeon-rev	TATAGGCGCGCCTCAACCTCCTTTATAGAG	*mNeongreen*
MurJ-for	ACTCGGCTAGCATGAGTGAAAGTAAAG	*murJ*
MurJ-rev	CTGTACCCGGGTGATCGTAAAAACCTAAC	*murJ*
PBP4_NheI-FW	GCGCGGCTAGCATGAAAAATTTAATATCTATTATCATC	*pbpD*
PBP4_SpeI-RV	GCGCGACTAGTTTTTCTTTTTCTAAATAAACGATTG	*pbpD*
YFP_SpeI_pCQ11_Ct-FW	CGCGACTAGTATGGTGAGCAAGGGCGAG	*yfp*
YFP_AscI_pCQ11_Ct-RV	GCGCGGGCGCGCCTCAGGCCTCTTGTACAGCC	*yfp*
RodA-c-v pMAD-5´	ACTGTATCAAATGGGATCCATCAATTCAT	*rodA*
RodA-c-v pMAD-3´	ATAGTTTAAAACGCGTACTTTTTGGATGGT	*rodA*
RodA-c-h pMAD-5	TCCAAAAAGTGAATTCTTTAAACTATTTTG	*downstream fragment of rodA*
RodA-c-h pMAD-3	TAGAGTGCGCTATAGATCTTAATTTTG	*downstream fragment of rodA*

Table S2.

Number of replicates and individual cells per replicate (if applicable) for all datasets shown in this study.

figure	subfigure	sample	No. of biological replicates	No. of cells replicate #1	No. of cells replicate #2	No. of cells replicate #3
1	b,c	CTRL	3	210	161	652
		VAN	3	274	354	132
		TELA	3	437	318	189
		OXA	3	487	213	237
	e	CTRL	3	57	77	46
		VAN	3	63	179	59
		TELA	3	72	121	121
		OXA	3	75	150	116
	h	CTRL	3	200	268	745
		VAN	3	402	182	819
		TELA	3	446	595	734
		OXA	3	494	377	306
2	c	CTRL full cycle (untreated assembly)	3	35	31	30

	b	CTRL cell phenotype %	3	134	131	131
	d	CTRL early	3	29	31	30
		CTRL mid	3	30	29	31
		CTRL late	3	30	32	30
3	b	VAN assembly	3	31	30	31
		VAN early	3	28	31	31
		VAN mid	3	30	31	31
		VAN late	3	32	31	31
		TELA assembly	3	30	31	31
		TELA early	3	31	31	31
		TELA mid	3	30	31	31
		TELA late	3	31	28	31
	c	CTRL 10 min	3	124	123	121
		VAN 10 min	3	121	123	124
		TELA10 min	3	122	121	124
		CTRL 70 min	3	124	123	121
		VAN 70 min	3	121	123	124
		TELA 70 min	3	122	121	124
4	a	OXA assembly	3	31	30	31
		OXA early	3	31	30	31
		OXA mid	3	30	30	31

		OXA late	3	30	31	31
	c	CTRL early	3	29	31	30
		CTRL mid	3	30	29	31
		CTRL late	3	30	32	30
		OXA early	3	31	30	31
		OXA mid	3	30	30	31
		OXA late	3	30	31	31
	d	CTRL mid	3	30	29	31
		CTRL late	3	30	32	30
		OXA mid	3	30	30	31
		OXA late	3	30	31	31
5	b,c	FtsW CTRL	3	333	185	170
		FtsW VAN	3	164	184	287
		FtsW TELA	3	327	226	263
		FtsW OXA	3	213	342	475
		RodA CTRL	3	856	380	689
		RodA VAN	3	302	400	468
		RodA TELA	3	504	404	879
		RodA OXA	3	421	647	511
		MurJ CTRL	3	402	293	343
		MurJ VAN	3	401	374	358
		MurJ TELA	3	401	373	320
		MurJ OXA	3	243	356	344

		PBP4 CTRL	3	157	221	165
		PBP4 VAN	3	130	323	994
		PBP4 TELA	3	390	170	400
		PBP4 OXA	3	626	423	489
		PBP2 CTRL	3	149	174	351
		PBP2 VAN	3	228	174	238
		PBP2 TELA	3	223	94	609
		PBP2 OXA	3	420	290	276
6	a	CTRL	3	149	174	351
		VAN	3	228	174	238
		TELA	3	223	94	609
		OXA	3	420	290	276
	b	CTRL	3	30	30	30
		OXA	3	30	30	30
	c	CTRL	3	30	30	30
		OXA	3	30	30	30
S1	b,c,d	MurJ	1	400	400	400
	e,f	FtsZ	3	210	161	652
S2	FtsZ	CTRL	3	210	161	652
		VAN	3	274	354	132
		TELA	3	437	318	189
		OXA	3	487	213	237
S3	FtsZ	CTRL	3	210	161	652

		VAN	3	274	354	132
		TELA	3	437	318	189
		OXA	3	487	213	237
	FtsW	CTRL	3	333	185	170
		VAN	3	164	184	287
		TELA	3	327	226	263
		OXA	3	213	342	475
	RodA	CTRL	3	856	380	689
		VAN	3	302	400	468
		TELA	3	504	404	879
		OXA	3	421	647	511
	MurJ	CTRL	3	402	293	343
		VAN	3	401	374	358
		TELA	3	401	373	320
		OXA	3	243	356	344
	PBP4	CTRL	3	157	221	165
		VAN	3	130	323	994
		TELA	3	390	170	400
		OXA	3	626	423	489
	PBP2	CTRL	3	149	174	351
		VAN	3	228	174	238
		TELA	3	223	94	609

		OXA	3	420	290	276
S4		CTRL	3	30	30	30
		VAN	3	30	30	30
		TELA	3	30	30	30
		OXA	3	30	30	30
S5		CTRL	3	-	-	-
		VAN	3	-	-	-
		TELA	3	-	-	-
		OXA	3	-	-	-
S6	a,b	CTRL	3	183	179	217
		VAN	3	175	361	457
		TELA	3	480	201	256
		NIS	3	229	180	154
	c	CTRL	3	-	-	-
		VAN	3	-	-	-
		TELA	3	-	-	-
		VAN	3	-	-	-

REFERENCES AND NOTES

1. M. G. Pinho, M. Kjos, J.-W. Veening, How to get (a)round: Mechanisms controlling growth and division of coccoid bacteria. *Nat. Rev. Microbiol.* **11**, 601–614 (2013).

2. D.-J. Scheffers, M. G. Pinho, Bacterial cell wall synthesis: New insights from localization studies. *Microbiol. Mol. Biol. Rev.* **69**, 585–607 (2005).

3. F. A. Rubino, A. Mollo, S. Kumar, E. K. Butler, N. Ruiz, S. Walker, D. E. Kahne, Detection of transport intermediates in the peptidoglycan flippase MurJ identifies residues essential for conformational cycling. *J. Am. Chem. Soc.* **142**, 5482–5486 (2020).

4. F. A. Rubino, S. Kumar, N. Ruiz, S. Walker, D. E. Kahne, Membrane potential is required for MurJ function. *J. Am. Chem. Soc.* **140**, 4481–4484 (2018).

5. S. F. F. Pereira, A. O. Henriques, M. G. Pinho, H. de Lencastre, A. Tomasz, Role of PBP1 in cell division of Staphylococcus aureus. *J. Bacteriol.* **189**, 3525–3531 (2007).

6. M. G. Pinho, S. R. Filipe, H. de Lencastre, A. Tomasz, Complementation of the essential peptidoglycan transpeptidase function of penicillin-binding protein 2 (PBP2) by the drug resistance protein PBP2A in Staphylococcus aureus. *J. Bacteriol.* **183**, 6525–6531 (2001).

7. J. M. Monteiro, A. R. Pereira, N. T. Reichmann, B. M. Saraiva, P. B. Fernandes, H. Veiga, A. C. Tavares, M. Santos, M. T. Ferreira, V. Macário, M. S. VanNieuwenhze, S. R. Filipe, M. G. Pinho, Peptidoglycan synthesis drives an FtsZ-treadmilling-independent step of cytokinesis. *Nature* **554**, 528–532 (2018).

8. T. Schneider, H.-G. Sahl, An oldie but a goodie - Cell wall biosynthesis as antibiotic target pathway. *Int. J. Med. Microbiol.* **300**, 161–169 (2010).

9. J. M. Ghuysen, Molecular structures of penicillin-binding proteins and β-lactamases. *Trends Microbiol.* **2**, 372–380 (1994).

10. F. Grein, T. Schneider, H.-G. Sahl, Docking on lipid II-A widespread mechanism for potent bactericidal activities of antibiotic peptides. *J. Mol. Biol.* **431**, 3520–3530 (2019).

11. P. E. Reynolds, Structure, biochemistry and mechanism of action of glycopeptide antibiotics. *Eur. J. Clin. Microbiol. Infect. Dis.* **8**, 943–950 (1989).

12. B. Salamaga, L. Kong, L. Pasquina-Lemonche, L. Lafage, M. von zur Und Zur Muhlen, J. F. Gibson, D. Grybchuk, A. K. Tooke, V. Panchal, E. J. Culp, E. Tatham, M. E. O'Kane, T. E. Catley, S. A. Renshaw, G. D. Wright, P. Plevka, P. A. Bullough, A. Han, J. K. Hobbs, S. J. Foster, Demonstration of the role of cell wall homeostasis in *Staphylococcus aureus* growth and the action of bactericidal antibiotics. *Proc. Natl. Acad. Sci. U.S.A.* **118** e2106022118 (2021).

13. M. A. Kohanski, D. J. Dwyer, J. J. Collins, How antibiotics kill bacteria: From targets to networks. *Nat. Rev. Microbiol.* **8**, 423–435 (2010).

14. M. G. Pinho, J. Errington, Recruitment of penicillin-binding protein PBP2 to the division site of Staphylococcus aureus is dependent on its transpeptidation substrates. *Mol. Microbiol.* **55**, 799–807 (2005).

15. X. Yang, R. McQuillen, Z. Lyu, P. Phillips-Mason, A. de La Cruz, J. W. McCausland, H. Liang, K. E. DeMeester, C. C. Santiago, C. L. Grimes, P. de Boer, J. Xiao, A two-track model for the spatiotemporal coordination of bacterial septal cell wall synthesis revealed by single-molecule imaging of FtsW. *Nat. Microbiol.* **6**, 584–593 (2021).

16. A. J. F. Egan, W. Vollmer, The physiology of bacterial cell division. *Ann. N. Y. Acad. Sci.* **1277**, 8–28 (2013).

17. R. McQuillen, J. Xiao, Insights into the structure, function, and dynamics of the bacterial cytokinetic FtsZ-Ring. *Annu. Rev. Biophys.* **49**, 309–341 (2020).

18. A. J. Perez, Y. Cesbron, S. L. Shaw, J. Bazan Villicana, H.-C. T. Tsui, M. J. Boersma, Z. A. Ye, Y. Tovpeko, C. Dekker, S. Holden, M. E. Winkler, Movement dynamics of divisome proteins and PBP2x:FtsW in cells of *Streptococcus pneumoniae*. *Proc. Natl. Acad. Sci. U.S.A.* **116**, 3211–3220 (2019).

19. V. A. Lund, K. Wacnik, R. D. Turner, B. E. Cotterell, C. G. Walther, S. J. Fenn, F. Grein, A. J. Wollman, M. C. Leake, N. Olivier, A. Cadby, S. Mesnage, S. Jones, S. J. Foster, Molecular coordination of *Staphylococcus aureus* cell division. *eLife* **7,** e32057 (2018).

20. X. Yang, Z. Lyu, A. Miguel, R. McQuillen, K. C. Huang, J. Xiao, GTPase activity-coupled treadmilling of the bacterial tubulin FtsZ organizes septal cell wall synthesis. *Science* **355**, 744–747 (2017).

21. A. W. Bisson-Filho, Y.-P. Hsu, G. R. Squyres, E. Kuru, F. Wu, C. Jukes, Y. Sun, C. Dekker, S. Holden, M. S. VanNieuwenhze, Y. V. Brun, E. C. Garner, Treadmilling by FtsZ filaments drives peptidoglycan synthesis and bacterial cell division. *Science* **355**, 739–743 (2017).

22. M. Pazos, K. Peters, M. Casanova, P. Palacios, M. VanNieuwenhze, E. Breukink, M. Vicente, W. Vollmer, Z-ring membrane anchors associate with cell wall synthases to initiate bacterial cell division. *Nat. Commun.* **9**, 5090 (2018).

23. N. Baranova, P. Radler, V. M. Hernández-Rocamora, C. Alfonso, M. López-Pelegrín, G. Rivas, W. Vollmer, M. Loose, Diffusion and capture permits dynamic coupling between treadmilling FtsZ filaments and cell division proteins. *Nat. Microbiol.* **5**, 407–417 (2020).

24. G. R. Squyres, M. J. Holmes, S. R. Barger, B. R. Pennycook, J. Ryan, V. T. Yan, E. C. Garner, Single-molecule imaging reveals that Z-ring condensation is essential for cell division in *Bacillus subtilis*. *Nat. Microbiol.* **6**, 553–562 (2021).

25. K. D. Whitley, C. Jukes, N. Tregidgo, E. Karinou, P. Almada, Y. Cesbron, R. Henriques, C. Dekker, S. Holden, FtsZ treadmilling is essential for Z-ring condensation and septal constriction initiation in *Bacillus subtilis* cell division. *Nat. Commun.* **12**, 2448 (2021).

26. S. F. F. Pereira, A. O. Henriques, M. G. Pinho, H. de Lencastre, A. Tomasz, Evidence for a dual role of PBP1 in the cell division and cell separation of Staphylococcus aureus. *Mol. Microbiol.* **72**, 895–904 (2009).

27. N. T. Reichmann, A. C. Tavares, B. M. Saraiva, A. Jousselin, P. Reed, A. R. Pereira, J. M. Monteiro, R. G. Sobral, M. S. VanNieuwenhze, F. Fernandes, M. G. Pinho, SEDS-bPBP pairs direct lateral and septal peptidoglycan synthesis in Staphylococcus aureus. *Nat. Microbiol.* **4**, 1368–1377 (2019).

28. K. Wacnik, V. A. Rao, X. Chen, L. Lafage, M. Pazos, S. Booth, W. Vollmer, J. K. Hobbs, R. J. Lewis, S. J. Foster, Penicillin-binding protein 1 (PBP1) of Staphylococcus aureus has multiple essential functions in cell division. *MBio* **13**, e0066922 (2022).

29. J. M. Monteiro, P. B. Fernandes, F. Vaz, A. R. Pereira, A. C. Tavares, M. T. Ferreira, P. M. Pereira, H. Veiga, E. Kuru, M. S. VanNieuwenhze, Y. V. Brun, S. R. Filipe, M. G. Pinho, Cell shape dynamics during the staphylococcal cell cycle. *Nat. Commun.* **6**, 8055 (2015).

30. B. M. Saraiva, M. Sorg, A. R. Pereira, M. J. Ferreira, L. C. Caulat, N. T. Reichmann, M. G. Pinho, Reassessment of the distinctive geometry of *Staphylococcus aureus* cell division. *Nat. Commun.* **11**, 4097 (2020).

31. G. K. Best, N. H. Best, A. V. Koval, Evidence for participation of autolysins in bactericidal action of oxacillin on Staphylococcus aureus. *Antimicrob. Agents Chemother.* **6**, 825–830 (1974).

32. G. Sakoulas, G. M. Eliopoulos, V. G. Fowler Jr., R. C. Moellering Jr., R. P. Novick, N. Lucindo, M. R. Yeaman, A. S. Bayer, Reduced susceptibility of Staphylococcus aureus to vancomycin and platelet microbicidal protein correlates with defective autolysis and loss of accessory gene regulator (agr) function. *Antimicrob. Agents Chemother.* **49**, 2687–2692 (2005).

33. M. A. Kohanski, D. J. Dwyer, B. Hayete, C. A. Lawrence, J. J. Collins, A common mechanism of cellular death induced by bactericidal antibiotics. *Cell* **130**, 797–810 (2007).

34. M. Osawa, H. P. Erickson, Liposome division by a simple bacterial division machinery. *Proc. Natl. Acad. Sci. U.S.A.* **110**, 11000–11004 (2013).

35. P. Szwedziak, Q. Wang, T. A. M. Bharat, M. Tsim, J. Löwe, Architecture of the ring formed by the tubulin homologue FtsZ in bacterial cell division. *eLife* **3**, e04601 (2014).

36. H. P. Erickson, D. E. Anderson, M. Osawa, FtsZ in bacterial cytokinesis: Cytoskeleton and force generator all in one. *Microbiol. Mol. Biol. Rev.* **74**, 504–528 (2010).

37. L. T. Nguyen, C. M. Oikonomou, G. J. Jensen, Simulations of Proposed Mechanisms of FtsZ-Driven Cell Constriction. *J. Bacteriol.* **203,** 3 (2021).

38. L. T. Nguyen, C. M. Oikonomou, H. J. Ding, M. Kaplan, Q. Yao, Y.-W. Chang, M. Beeby, G. J. Jensen, Simulations suggest a constrictive force is required for Gram-negative bacterial cell division. *Nat. Commun.* **10**, 1259 (2019).

39. C. Coltharp, J. Buss, T. M. Plumer, J. Xiao, Defining the rate-limiting processes of bacterial cytokinesis. *Proc. Natl. Acad. Sci. U.S.A.* **113**, E1044–E1053 (2016).

40. V. R. Steele, A. L. Bottomley, J. Garcia-Lara, J. Kasturiarachchi, S. J. Foster, Multiple essential roles for EzrA in cell division of Staphylococcus aureus. *Mol. Microbiol.* **80**, 542–555 (2011).

41. S. Schenk, R. A. Laddaga, Improved method for electroporation of *Staphylococcus aureus*. *FEMS Microbiol. Lett.* **94**, 133–138 (1992).

42. F. Grein, A. Müller, K. M. Scherer, X. Liu, K. C. Ludwig, A. Klöckner, M. Strach, H.-G. Sahl, U. Kubitscheck, T. Schneider, Ca^{2+}-daptomycin targets cell wall biosynthesis by forming a tripartite complex with undecaprenyl-coupled intermediates and membrane lipids. *Nat. Commun.* **11**, 1455 (2020).

43. M. Tokunaga, N. Imamoto, K. Sakata-Sogawa, Highly inclined thin illumination enables clear single-molecule imaging in cells. *Nat. Methods* **5**, 159–161 (2008).

44. D. Sage, L. Donati, F. Soulez, D. Fortun, G. Schmit, A. Seitz, R. Guiet, C. Vonesch, M. Unser, DeconvolutionLab2: An open-source software for deconvolution microscopy. *Methods* **115**, 28–41 (2017).

45. C. A. Schneider, W. S. Rasband, K. W. Eliceiri, NIH Image to ImageJ: 25 years of image analysis. *Nat. Methods* **9**, 671–675 (2012).

46. H. Kirshner, F. Aguet, D. Sage, M. Unser, 3-D PSF fitting for fluorescence microscopy: Implementation and localization application. *J. Microsc.* **249**, 13–25 (2013).

47. J. D. Te Winkel, D. A. Gray, K. H. Seistrup, L. W. Hamoen, H. Strahl, Analysis of antimicrobial-triggered membrane depolarization using voltage sensitive dyes. *Front. Cell Dev. Biol.* **4**, 29 (2016).

48. I. Wiegand, K. Hilpert, R. E. W. Hancock, Agar and broth dilution methods to determine the minimal inhibitory concentration (MIC) of antimicrobial substances. *Nat. Protoc.* **3**, 163–175 (2008).

49. A. Ducret, E. M. Quardokus, Y. V. Brun, MicrobeJ, a tool for high throughput bacterial cell detection and quantitative analysis. *Nat. Microbiol.* **1**, 16077 (2016).

50. S. J. Lord, K. B. Velle, R. D. Mullins, L. K. Fritz-Laylin, SuperPlots: Communicating reproducibility and variability in cell biology. *J. Cell Biol.* **219,** e202001064 (2020).

51. J. Schindelin, I. Arganda-Carreras, E. Frise, V. Kaynig, M. Longair, T. Pietzsch, S. Preibisch, C. Rueden, S. Saalfeld, B. Schmid, J.-Y. Tinevez, D. J. White, V. Hartenstein, K. Eliceiri, P. Tomancak, A. Cardona, Fiji: An open-source platform for biological-image analysis. *Nat. Methods* **9**, 676–682 (2012).

52. P. P. Navarro, A. Vettiger, V. Y. Ananda, P. M. Llopis, C. Allolio, T. G. Bernhardt, L. H. Chao, Cell wall synthesis and remodelling dynamics determine division site architecture and cell shape in Escherichia coli. *Nat. Microbiol.* **7**, 1621–1634 (2022).

53. C. S. Lunde, S. R. Hartouni, J. W. Janc, M. Mammen, P. P. Humphrey, B. M. Benton, Telavancin disrupts the functional integrity of the bacterial membrane through targeted interaction with the cell wall precursor lipid II. *Antimicrob. Agents Chemother.* **53**, 3375–3383 (2009).

54. H. Strahl, L. W. Hamoen, Membrane potential is important for bacterial cell division. *Proc. Natl. Acad. Sci. U.S.A.* **107**, 12281–12286 (2010).

55. M. B. Tol, D. Morales Angeles, D.-J. Scheffers, In vivo cluster formation of nisin and lipid II is correlated with membrane depolarization. *Antimicrob. Agents Chemother.* **59**, 3683–3686 (2015).

56. B. N. Kreiswirth, S. Löfdahl, M. J. Betley, M. O'Reilly, P. M. Schlievert, M. S. Bergdoll, R. P. Novick, The toxic shock syndrome exotoxin structural gene is not detectably transmitted by a prophage. *Nature* **305**, 709–712 (1983).

57. S. Herbert, A.-K. Ziebandt, K. Ohlsen, T. Schäfer, M. Hecker, D. Albrecht, R. Novick, F. Götz, Repair of global regulators in Staphylococcus aureus 8325 and comparative analysis with other clinical isolates. *Infec. Immun.* **78**, 2877–2889 (2010).